J|A|C|S ARTICLES

Published on Web 04/20/2010

"Magnet-in-the-Semiconductor" FePt−PbS and FePt−PbSe Nanostructures: Magnetic Properties, Charge Transport, and Magnetoresistance

Jong-Soo Lee,[†] Maryna I. Bodnarchuk,[†,§] Elena V. Shevchenko,[‡] and Dmitri V. Talapin*[,†,‡]

Department of Chemistry, University of Chicago, Chicago, Illinois 60637 and Center for Nanoscale Materials, Argonne National Laboratory, Argonne, Illinois 60439

Received January 6, 2010; E-mail: dvtalapin@uchicago.edu

Abstract: We report a synthesis of colloidal nanostructures combining a magnetic material (FePt) with a narrow-gap semiconductor (PbS and PbSe) in form of core−shells or nanodumbbells and explore their optical, magnetic, electrical, and magnetotransport properties. The arrays of "magnet-in-the-semiconductor" nanostructures show semiconductor-type transport properties with magnetoresistance typical for magnetic tunnel junctions, thus combining the advantages of both functional components. We observed gate-controlled charge transport through the arrays of FePt−PbS and FePt−PbSe core−shell nanostructures with an electron mobility of 0.01 $cm^2/(V\ s)$ and 0.08 $cm^2/(V\ s)$, respectively, combined with ferro- and superparamagnetic behavior and large tunneling magnetoresistance. This work shows that multicomponent colloidal nanostructures can be used as the building blocks for design of multifunctional materials for electronics and optoelectronics.

1. Introduction

In recent years colloidal synthesis of inorganic nanomaterials has developed into a powerful branch of synthetic chemistry.[1] Size- and shape-controlled nanoparticles of metals, semiconductors, and magnetic materials[2,3] as well as different multicomponent structures combining two- or more functional components (e.g., a metal and a semiconductor) can be synthesized with a level of structural precision currently not achievable for top-down techniques. These colloidal nanostructures can be obtained in macroscopic quantities at the price of conventional chemical compounds, providing a powerful route toward novel man-made materials with different functionalities complementing each other and ultimately creating novel synergistic effects.

Colloidal semiconductor nanocrystals (NCs) are considered promising candidates for device applications[4] including light-emitting devices,[5] solar cells,[6,7] field-effect transistors,[8,9] and photodetectors.[10] Introducing ways of controlling and manipulating the spins, in addition to charges, would provide opportunities for development of NC-based spintronic[11] and memory applications.[12] Recently it has been shown that NCs of dilute magnetic semiconductors (DMS) can exhibit remarkable properties, such as spontaneous magnetization of dopands by light[13] or charging.[14] These effects, not observable in bulk DMS, become possible in CdSe and ZnO NCs doped with magnetic Mn^{2+} ions because of tight spatial confinement of semiconductor wave functions in proximity to magnetic impurities leading to stronger interactions of charge carriers with the magnetic dopands.

In this work we synthesized and studied the nanostructures combining ferromagnetic NCs with quantum-confined semiconductors. In such systems, compared to bulk heterostructures, the intercomponent interactions should be substantially forced by the tight spatial confinement, which may affect the electronic structure through, e.g., Zeeman splitting of quantum confined states in a semiconductor under local magnetic field. In addition, the exchange of charge carriers between ferromagnetic and semiconducting phases should induce spin polarization in a nonmagnetic semiconductor caused by the injection of spins from the ferromagnetic phase.[15,16]

[†] University of Chicago.
[‡] Argonne National Laboratory.
[§] On leave from the Institute of Semiconductor and Solid State Physics, Johannes Kepler University Linz, A-4040 Linz, Austria.

(1) Yin, Y.; Alivisatos, A. P. *Nature* **2005**, *437*, 664–670.
(2) Burda, C.; Chen, X.; Narayanan, R.; El-Sayed, M. A. *Chem. Rev.* **2005**, *105*, 1025–1102.
(3) Sun, S.; Murray, C. B.; Weller, D.; Folks, L.; Moser, A. *Science* **2000**, *287*, 1989–1992.
(4) Talapin, D. V.; Lee, J.-S.; Kovalenko, M. V.; Shevchenko, E. V. *Chem. Rev.* **2010**, *110*, 389–458.
(5) Caruge, J. M.; Halpert, J. E.; Wood, V.; Bulovic, V.; Bawendi, M. G. *Nat. Photonics* **2008**, *2*, 247–250.
(6) Luther, J. M.; Law, M.; Beard, M. C.; Song, Q.; Reese, M. O.; Ellingson, R. J.; Nozik, A. J. *Nano Lett.* **2008**, *8*, 3488–3492.
(7) Gur, I.; Fromer, N. A.; Geier, M. L.; Alivisatos, A. P. *Science* **2005**, *310*, 462–465.
(8) Talapin, D. V.; Murray, C. B. *Science* **2005**, *310*, 86–89.
(9) Sun, B.; Sirringhaus, H. *J. Am. Chem. Soc.* **2006**, *128*, 16231–16237.
(10) Konstantatos, G.; Howard, I.; Fischer, A.; Hoogland, S.; Clifford, J.; Klem, E.; Levina, L.; Sargent, E. H. *Nature* **2006**, *442*, 180–183.
(11) Žutić, I.; Fabian, J.; Das Sarma, S. *Rev. Mod. Phys.* **2004**, *76*, 323–410.
(12) Chappert, C.; Fert, A.; Van Dau, F. N. *Nat. Mater.* **2007**, *6*, 813–823.
(13) Beaulac, R.; Schneider, L.; Archer, P. I.; Bacher, G.; Gamelin, D. R. *Science* **2009**, *325*, 973–976.
(14) Ochsenbein, S. T.; Feng, Y.; Whitaker, K. M.; Badaeva, E.; Liu, W. K.; Li, X.; Gamelin, D. R. *Nat. Nanotechnol.* **2009**, *4*, 681–687.
(15) Hanbicki, A. T.; Jonker, B. T.; Itskos, G.; Kioseoglou, G.; Petrou, A. *Appl. Phys. Lett.* **2002**, *80*, 1240–1242.

10.1021/ja100029s

Several hybrid nanostructures combining metal and semiconductor components have been synthesized in the past years: FePt−CdS dumbbells,[13] CdSe nanorods with Au[17] and Co tips,[18] Au−PbS[19] and FePt−ZnO core−shells,[20] etc. As examples of synergistic effects observed in such structures, Millo et al. reported the observation of the subgap structure in Au−CdSe−Au nanorods;[21] p-type doping was observed in films of Au−PbS core−shell NCs due to the intraparticle charge transfer between Au core and PbS shell.[19] In this work we synthesized and studied nanostructures combining FePt with lead chalcogenides (PbS and PbSe). This choice of magnetic component was motivated by good chemical stability and well-understood magnetic properties of FePt NCs,[3] while PbS and PbSe NCs have demonstrated the best electrical performance in terms of conductivity and carrier mobility in NC arrays.[8,19,22]

2. Experimental Section

Synthesis of Cubic FePt−PbS Core−Shell Nanostructures. FePt NCs were synthesized utilizing a slightly modified method of Sun et al.[3] (see Supporting Information). In a typical preparation, 0.225 g of PbO and 5 mL of oleic acid were dissolved in 5 mL of 1-octadecene (ODE). The mixture was heated to 140 °C for 1 h under vacuum to form a lead oleate complex. After the obtained clear solution was cooled to 120 °C under nitrogen, FePt nanoparticles (e.g., 3.8 nm, 4 mg) dissolved in 0.4 mL of toluene were injected under nitrogen gas flow and toluene was distilled off under vacuum. For the growth of the PbS shell, 0.13 mL of bis(trimethylsilyl)sulfide (TMS_2S) dissolved in 2 mL of ODE was rapidly injected into the reaction mixture at 150 °C under vigorous stirring. The reaction mixture was kept at 150 °C for 5−10 min to obtain the desired PbS shell thickness and then quickly cooled using a water bath. After the mixture cooled to room temperature, the nanoparticles were precipitated from the crude solution by addition of hexane/ethanol (3:1) followed by centrifugation. Precipitated nanocrystals were redissolved in hexane (∼5 mL) and precipitated again with ethanol. Precipitated nanoparticles were transferred to a nitrogen-filled glovebox and redispersed in anhydrous chloroform. As-synthesized FePt−PbS nanostructures had narrow size and shape distributions confirmed by TEM and SAXS studies and were used without postpreparative size selection.

Synthesis of FePt−PbSe Nanostrucures. 0.446 g of PbO and 1.5 mL of oleic acid were dissolved in 8 mL of ODE. This mixture was heated to 150 °C for 1 h under vacuum to form a lead oleate complex. After cooling the mixture to 120 °C under nitrogen, FePt nanoparticles (3.8 nm, 4 mg) in 0.4 mL of toluene were injected under nitrogen gas flow and toluene was distilled off. For the growth of the PbSe shell, 3 mL of 1 M trioctylphosphine selenide were rapidly injected into the reaction mixture at 170 °C under vigorous stirring. The reaction mixture was kept at 160 °C for 10 min and then quickly cooled using a water bath. After the mixture cooled to room temperature, the nanoparticles were precipitated from the crude solution by addition of hexane/ethanol (3:1) followed by centrifugation. Precipitated nanocrystals were redissolved in hexane (∼5 mL) and precipitated again with ethanol. The precipitated nanoparticles were transferred to a nitrogen-filled glovebox and redispersed in anhydrous chloroform.

Structural, Magnetic, and Electrical Characterization of FePt−PbS and FePt−PbSe Nanostructures. Samples for TEM characterization were prepared by placing 1−2 μL of a diluted (0.1 mg/mL) solution in toluene or tetrachloroethylene on a carbon-coated copper grid (Ted-Pella). The excess solvent was removed after 10 s with a filter paper. TEM and HRTEM images were obtained using a FEI Tecnai F30 field emission analytical transmission electron microscope operating at an acceleration voltage of 300 kV. Wide-angle powder X-ray diffraction patterns were collected using a Bruker D8 powder diffractometer with a Cu K_a radiation source and VANTEC 2000 area detector.

Samples for electrical measurements were prepared by depositing an ∼100 nm thick film of close-packed FePt−PbX (X = S, Se) nanostructures by drop casting extensively purified colloidal solutions in a hexane/octane (∼9:1 vol.) mixture on highly doped Si wafers with a 110 nm thick SiO_2 thermal gate oxide. Source and drain Ti/Au (70/450 Å) electrodes were lithographically patterned on the SiO_2 surface prior to the deposition of colloidal nanostructures. Close-packed FePt−PbX (X = S, Se) nanostructure films were treated with hydrazine by dipping the wafers into a 1.0 M solution of hydrazine in anhydrous acetonitrile. Duration of the treatment varied from 12 to 24 h, followed by rinsing the device with anhydrous acetonitrile. The hydrazine-treated films were insoluble in common solvents such as hexane and chloroform. Freshly hydrazine-treated NC films were dried at 70 °C for 30 min under nitrogen. Due to reduction in interparticle spacing, treated NC films exhibited some cracks. To further improve the electrical conductivity these cracks could be filled in by adding fresh FePt−PbX (X = S, Se) nanostructures. Additional FePt−PbX (X = S, Se) solution was cast on top of the hydrazine treated film. After depositing the second layer and drying, the hydrazine treatment was repeated. Field-effect devices were tested using an Agilent B1500 semiconductor parameter analyzer. All room temperature electrical measurements were performed under a dry nitrogen atmosphere.

Magnetic properties were studied using SQUID magnetometry (MPMS XL, Quantum Design). Zero-field-cooled (ZFC) and field-cooled (FC) studies were recorded in the 5−300 K range at H = 100 Oe after cooling the samples in the absence or in the presence of a 100 Oe field, respectively. For magnetic measurements samples were prepared in the form of thoroughly washed and dried powders of FePt−PbX (X = S, Se) nanostructures.

Low temperature conductivity and magnetoresistance measurements were carried out using a Physical Property Measurement System (PPMS-9, Quantum Design). The NC films for magnetoresistance measurement were prepared similarly to the films for electrical measurements by drop casting extensively purified colloidal solutions in a hexane/octane (∼9:1 vol.) mixture on highly doped Si wafers with a 110 nm thick SiO_2 thermal gate oxide. Source and drain Ti/Au (70/450 Å) electrodes with a gap spacing of 5 μm lithographically patterned on the SiO_2 surface were wire bonded to connect the PPMS sample holder prior to the deposition of colloidal nanostructures. Close-packed FePt−PbX (X = S, Se) nanostructure films were treated with hydrazine for 24 h by dipping the wafers into a 1.0 M solution of hydrazine in anhydrous acetonitrile. The resistances were first measured at zero field while changing the temperature from 300 to 2 K. For magnetoresistance measurement, the magnetic field was applied parallel and perpendicular to the current flow. The magnetoresistance studies were carried out at different temperatures (2−60 K) with the field scanning from zero to +50 kOe then to −50 kOe and back to zero field. The drive current was changed between 200 nA and/or 1.5 μA, depending on sample resistance.

(16) Lou, X.; Adelmann, C.; Furis, M.; Crooker, S. A.; Palmstrom, C. J.; Crowell, P. A. *Phys. Rev. Lett.* **2006**, *96*, 176603–4.
(17) Mokari, T.; Rothenberg, E.; Popov, I.; Costi, R.; Banin, U. *Science* **2004**, *304*, 1787–1790.
(18) Maynadie, J.; Asaf, S.; Andrea, F.; Marc, R.; Ehud, S.; Uri, B.; Katerina, S.; Bruno, C. *Angew. Chem.* **2009**, *121*, 1846–1849.
(19) Lee, J. S.; Shevchenko, E. V.; Talapin, D. V. *J. Am. Chem. Soc.* **2008**, *130*, 9673–9675.
(20) Tiejun, Z.; Meihua, L.; Zhihua, Z.; Hao, G.; Wee Shong, C.; Bo, L. *Adv. Mater.* **2010**, *22*, 403–406.
(21) Steiner, D.; Mokari, T.; Banin, U.; Millo, O. *Phys. Rev. Lett.* **2005**, *95*, 056805.
(22) Law, M.; Luther, J. M.; Song, Q.; Hughes, B. K.; Perkins, C. L.; Nozik, A. J. *J. Am. Chem. Soc.* **2008**, *130*, 5974–5985.

3. Results and Discussion

Synthesis of FePt−PbX (X = S, Se) Nanostructures. For synthesis of FePt−PbS nanostructures, bis(trimethylsilyl) sulfide (further referred to as TMS_2S) was injected into the reaction mixture containing monodisperse FePt NCs, oleic acid, and a Pb-oleate complex dissolved in 1-octadecene. FePt NCs played the role of seeds for nucleation of the PbS phase whose morphology was controlled by the reaction temperature and by the ligands present at the surface of FePt NCs. The characteristic FePt−PbS nanostructures included dumbbells (Figures 1a and S1a) and core−shells with spherical (Figure S1b) or cubic (Figure 1b) PbS shell. Scheme 1 provides an illustration of the parameters controlling the nanostructure morphology. To obtain core−shell nanostructures, the surface of FePt cores, originally stabilized with oleic acid and oleylamine, has to be extensively treated with an excess of oleylamine. Such treatment with labile amine surfactants facilitated simultaneous nucleation of PbS at multiple sites at the surface of FePt seeds. At 100 °C PbS domains nucleated, grew, and eventually coalesced forming rather uniform polycrystalline PbS shells (Figure S1b). Increasing the growth temperature to 150 °C led to single-crystalline cubic PbS particles incorporating FePt cores (Figure 1b). High-resolution TEM studies confirmed the single-crystalline nature of the PbS shell, presumably formed *via* recrystallization of several domains. The shell thickness could be controlled by the reaction time, the concentration of FePt seeds, and the amount of injected sulfur precursor (Figure S2). Synthesis of dumbbell-like FePt−PbS nanostructures required extensive washing of FePt NCs from oleylamine ligands and recapping them with less labile oleate ligands (Figure 1a and Scheme 1). At 100 °C the reaction yielded dumbbell structures with near-spherical 8.5 nm PbS NCs attached to 3.5 nm FePt NCs (Figure S1a), while the dumbbells synthesized at 150 °C comprised spherical FePt and cubic PbS components (Figures 1a and S3). We did not observe evidence for an epitaxial relationship between FePt and PbS phases in nanodumbbells (Figure S3b−d).

The integration of FePt cores into PbS nanocrystals washes out the sharp excitonic features inherent to monodisperse PbS quantum dot samples (Figure 2a). This effect could be caused by either homogeneous or inhomogeneous spectral broadening. Careful analysis of TEM images and SAXS data (Figure S4) revealed low size inhomogeneity (<15% std dev) of FePt−PbS core−shell nanostructures, incomparable with the broadening observed in the absorption spectra. The homogeneous broadening of the excitonic peaks can be caused by their coupling to the continuum of electronic states in the metallic FePt core. The decay of the exciton generated in the PbS shell into the metallic core should satisfy the uncertainty principle $\delta\tau\ \delta E \geq \hbar/2$. If the transfer rate is very fast, in the femtosecond domain, δE causes the homogeneous broadening of the spectral lines. Similar homogeneous broadening has been observed in the absorption spectra of Au−PbS core−shell nanostructures.[19] When the metallic core is not directly integrated into the semiconductor lattice, but is attached in the form of an FePt−PbS dumbbell, a slower energy transfer is expected with smaller homogeneous broadening (Figure 2a).

Monodisperse and structurally uniform FePt−PbSe nanostructures (Figure 1c) were synthesized at 170 °C following the above-described approach while using tri-*n*-octylphosphine selenide as the selenium precursor. The typical morphology can be described as an intermediate case between a core−shell and a dumbbell; the nanostructures had a nearly spherical overall shape, but FePt cores were located not at the center, but close to the surface of PbSe NCs.

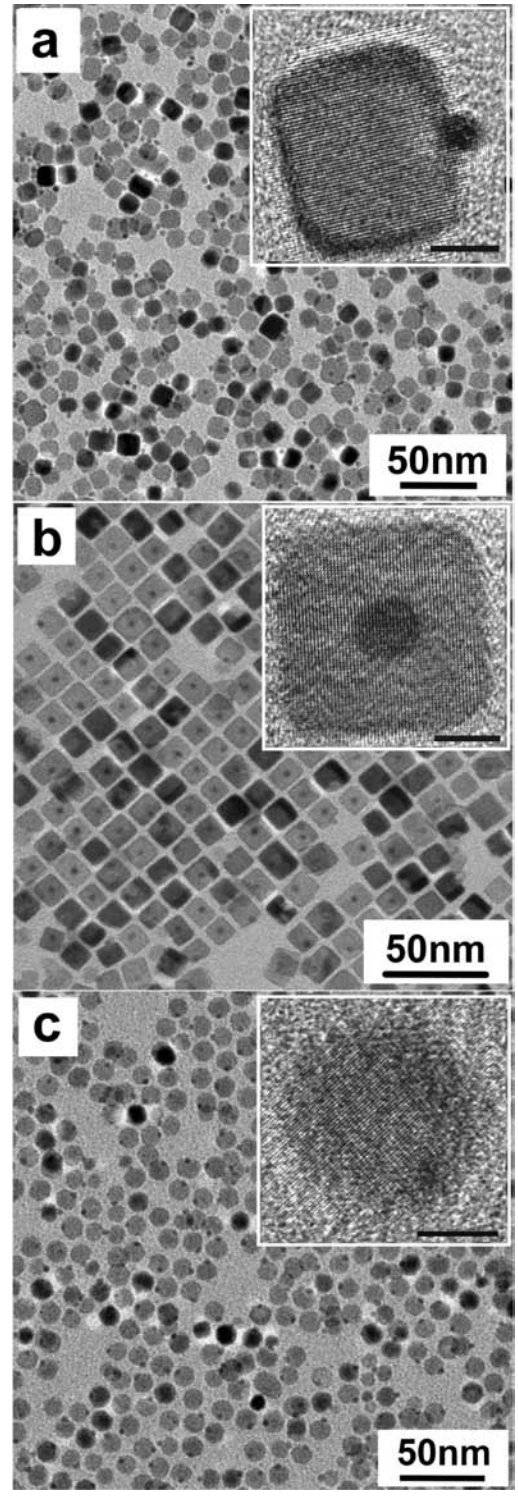

Figure 1. Transmission electron microscopy images of FePt−PbS nanostructures with (a) dumbbell and (b) cubic core−shell morphologies. (c) TEM image of FePt−PbSe nanostructures. The insets show high-resolution images with 5 nm scale bars.

Figure 2b compares powder X-ray diffraction patterns of FePt cores, cubic FePt−PbS core−shells, and FePt−PbSe nanostructures, revealing the presence of a chemically disordered *fcc* FePt phase (∼1:1 stoichiometry) in as-synthesized FePt NCs and FePt−PbX (X = S, Se) nanostructures. Both PbS and PbSe components crystallized in the rock-salt structure. The small

Scheme 1. Morphology-Directing Synthetic Conditions for FePt−PbS Nanostructures

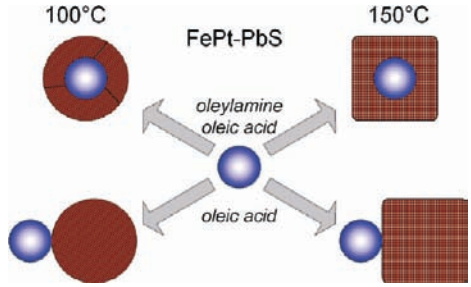

size of the FePt core compared to the PbSe shell resulted in weak and broad reflections from the FePt phase. The PbS and PbSe diffraction peaks matched the reflections of corresponding bulk phases (Figure 2b), showing that no lattice strain developed in the PbS and PbSe shells of core−shell nanostructures. The Scherrer analysis of the XRD patterns yielded 11.5 and 9.6 nm for PbS and PbSe crystalline domains in FePt−PbS and FePt−PbSe core−shells, respectively. These values were only slightly smaller than the sizes measured by TEM (Figure 1b,c), further confirming the excellent crystallinity of the lead chalcodenide shells, despite the absence of epitaxial relationships between the core and the shell.

Magnetic Properties of FePt−PbX (X = S, Se) Nanostructures. Figure 3a shows the magnetization versus applied-field (M vs H) hysteresis loops for a powder of as-prepared 3.5 nm

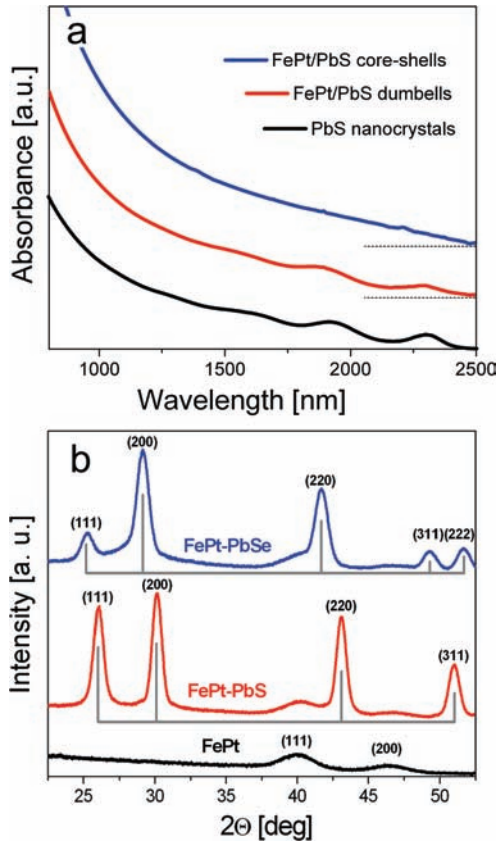

Figure 2. (a) Optical absorption spectra for colloidal solutions of PbS NCs, dumbbell-like FePt−PbS, and cubic core−shell FePt−PbS nanostructures dispersed in tetrachloroethylene. (b) Powder X-ray (Cu K_a radiation) diffraction patterns of FePt nanocrystals, cubic FePt−PbS core−shells, and FePt−PbSe nanostructures. Gray vertical lines indicate X-ray reflection positions and relative intensities for bulk PbS and PbSe phases.

fcc FePt NCs. At 5 K the NCs showed ferromagnetic behavior with the coercive field (H_c) ≈ 1.9 kOe. The shape of the hysteresis loop can be described using the Stoner−Wolfarth model modified to account for exchange interactions between closely packed neighboring NCs.[23] The blocking temperature (T_B), estimated from the maximum in ZFC scan (Figure 3d), was ∼15 K, typical for *fcc* phase FePt NCs with low intrinsic magnetocrystalline anisotropy.[3] At room temperature (300 K) FePt nanocrystals showed superparamagnetic behavior with $H_c = 0$ (Figure 3a, inset). We also observed a strong temperature dependence for saturation magnetization (M_0): 6.6 emu/g at 5 K vs 0.9 emu/g at 300 K, both measured at $H = 20$ kOe. Such behavior is usually associated with the disorder of surface spins gradually increasing with temperature.[24]

The formation of PbS shells resulted in significant changes in the magnetic properties. As expected, the formation of a nonmagnetic shell reduced M_0 per unit weight. At the same time, M_0 normalized to the content of the FePt phase in hybrid nanostructures did not reveal significant changes, suggesting that the number of exchange-coupled spins remained approximately the same. In addition, we observed a softening of the low-temperature magnetic response; H_c reduced to approximately 20 and 80 Oe at 5 K for FePt−PbS and FePt−PbSe nanostructures, respectively (Figure 3b,c). ZFC scans measured for FePt−PbS cubic core−shells revealed two peaks, one at 14 K, expected for the FePt core, and the second peak at ∼70 K (Figure 3d). When the PbS shell was grown at 100 °C, no second peak in the ZFC scan appeared (Figure S5).

The changes in the hysteresis loop combined with the appearance of a second peak in ZFC scans suggest the presence of two coupled magnetic phases in FePt−PbS nanostructures synthesized at 150 °C. A magnetically soft phase easily switches at low field while the hysteresis at higher fields indicates the response of a harder FePt phase. Similar behavior was reported, e.g., for FePt−Fe_2O_3 core−shell nanoparticles.[25] To find the origin of the soft magnetic response, we carried out control experiments using FePt NCs treated separately with Pb-oleate and TMS_2S under conditions identical to those used for the synthesis of FePt−PbS nanostructures. The treatment of FePt nanocrystals with Pb-oleate did not alter their magnetic properties (Figure S6a,b), whereas the effect of TMS_2S treatment at 150 °C was rather dramatic. We observed the appearance of a soft magnetic phase with $H_c \approx 20$ Oe at 5 K (Figure S6c) and two distinct peaks in ZFC scans at 15 and 230 K (Figure S6d). The treatment of FePt NCs with TMS_2S lowered the M_0 at 5 K by ∼30%, whereas the M_0 at 300 K more than doubled (cf. Figures 3a and S6c). The latter observation could evidence that the formation of Fe−S bonds at the FePt−PbS interface reduced the disorder of surface spins in *fcc* FePt nanocrystals at room temperature. Prolonged exposure of FePt NCs to TMS_2S at 150 °C resulted in the additional peaks in powder XRD patterns characteristic of the greigite Fe_3S_4, known to be a soft magnetic phase with a reported Curie temperature of 527 °C[26] (Figure S7b). When FePt NCs were treated with TMS_2S at 100 °C, no additional peaks in the XRD patterns were observed (Figure 6b).

Since the magnetic behavior of 3.5 nm FePt NCs treated with TMS_2S matched that of FePt−PbS nanostructures, we concluded

(23) Schrefl, T.; Hrkac, G.; Suess, D.; Scholz, W.; Fidler, J. *J. Appl. Phys.* **2003**, *93*, 7041–7043.
(24) Jang, S.; Kong, W.; Zeng, H. *Phys. Rev. B* **2007**, *76*, 212403.
(25) Liu, C.; Wu, X.; Klemmer, T.; Shukla, N.; Weller, D.; Roy, A. G.; Tanase, M.; Laughlin, D. *Chem. Mater.* **2005**, *17*, 620–625.
(26) Chang, L.; Roberts, A. P.; Tang, Y.; Rainford, B. D.; Muxworthy, A. R.; Chen, Q. *J. Geophys. Res.* **2008**, *113*, B06104.

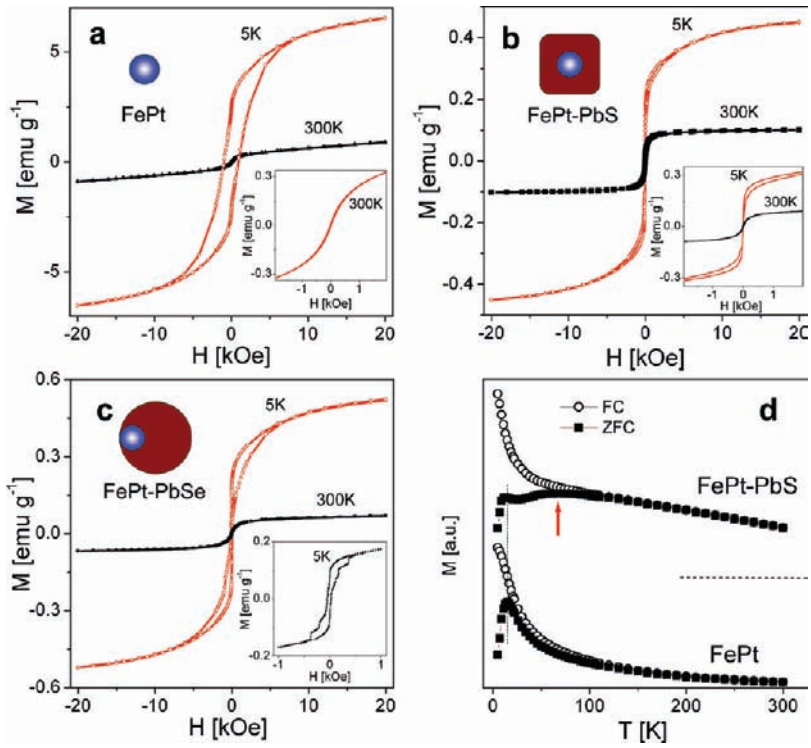

Figure 3. Magnetic properties of FePt and FePt−PbX (X = S, Se) nanostructures. Magnetization vs applied field hysteresis loops measured at 5 and 300 K for (a) 3.5 nm FePt nanocrystals, (b) FePt−PbS cubic core−shells with 3.5 nm FePt core and ∼4 nm thick PbS shell; (c) FePt−PbSe nanostructures with 3.5 nm FePt cores integrated into 12 nm PbSe nanocrystals. The insets show magnified views of the hysteresis loops at low-field. (d) Zero-field-cooled (ZFC) and field-cooled (FC) scans measured at $H = 100$ Oe for 3.5 nm FePt nanocrystals and for FePt−PbS core−shells with 3.5 nm FePt core and ∼4 nm thick PbS shell. Curves are vertically offset for clarity. Arrow shows the second peak in ZFC scan for FePt−PbS core−shells. The magnetization of all samples was normalized to the weight of entire nanostructures.

that a thin interfacial layer of iron−sulfide formed at the interface between the magnetic core and semiconducting shell and contributed to the magnetic response of our hybrid nanostructures. Similar behavior was observed in the case of FePt−PbSe nanostructures (Figures 3c and S8) where, in addition to the contribution of a soft component to the hysteresis loop, we observed reproducible stepwise magnetization steps in weak fields (Figure 3c, inset). Similar magnetization steps have been reported for exchange coupled epitaxial magnetic bilayers where magnetization reversal of each layer occurs at a characteristic field.[27] The synchronous switching of an ensemble of nanostructures implies well-defined interfaces formed between FePt and PbSe phases.

Gated Charge Transport in Arrays of FePt/PbS and FePt/PbSe Nanostructures. For charge transport studies we used field-effect transistor (FET) measurements in back-gate geometry with bottom Au electrodes (Figure 4a). Close packed NC films were deposited on FET substrates by spin-coating or dropcasting (Figure S9). All as-deposited films showed poor conductivity $G \approx 10^{-11}$ S cm^{-1} (Figure S10) due to the weak electronic coupling between individual nanostructures separated with bulky oleic acid capping ligands. To improve the conductivity, we treated the films with a 1 M solution of N_2H_4 in acetonitrile for 12 to 24 h. Such treatment is known to dramatically increase the conductivity of PbS and PbSe NC films without affecting NC size and shape.[8,19] Previous studies have shown that small hydrazine molecules replace bulky oleate groups at the NC surface thus decreasing the interparticle spacing from ∼1.4 nm to ∼0.4 nm.[8,22] In addition, highly polarizable hydrazine molecules help reduce the mismatch in dielectric constants at the NC surface, thus lowering the Coulomb charging energy in the NC solid.[8] It was also shown that hydrazine can inject electrons into the $1S_e$ quantum confined state of lead chalcogenide NCs behaving as an n-type charge-transfer dopand.[8]

After exposure to N_2H_4 solution, the conductivity of FePt−PbS and FePt−PbSe nanostructures increased by approximately 9 and 10 orders of magnitude, respectively. In both structures the current flowing between source and drain electrodes (I_D) could be modulated by applying voltage to the gate terminal (V_G). I_D increased with increasing V_G, typical for n-type conductivity through the FET channel (Figure 4c,d). The field effect mobility in the saturation regime (μ_{sat}) was estimated from the slope of the $I_D^{1/2}$ vs V_G plot (Figure 4d). For cubic FePt/PbS core−shells, μ_{sat} was ∼0.01 cm^2/(V s) and the ratio of currents in "on" and "off" states was $I_{on}/I_{off} \approx 60$ (Figure 4d). For n-FETs assembled from FePt/PbS dumbbell μ_{sat} was $\sim 3 \times 10^{-3}$ cm^2/(V s) with $I_{on}/I_{off} \approx 10^2$ (Figure S11). Higher conductance and mobility in the arrays of FePt/PbS core−shells compared to dumbbells could originate from a number of factors, including the higher packing density of core−shells compared to anisotropic nanodumbbells. The FET devices assembled from FePt/PbSe nanostructures also showed a stable n-type gate effect after N_2H_4 treatment. Compared to FETs on FePt−PbS core−shells, the FePt−PbSe FETs showed smaller $I_{on}/I_{off} \approx 5-10$ but almost an order of magnitude higher for on-currents (Figure 4e,f). The linear regime field effect mobility extracted from the transconductance was 0.08 cm^2 V^{-1} s^{-1}.

The observation of n-type transport in FePt−PbS nanostructures is rather counterintuitive. The reported work function of

(27) Suzuki, Y.; van Dover, R. B.; Gyorgy, E. M.; Phillips, J. M.; Felder, R. J. *Phys. Rev. B* **1996**, *53*, 14016–14019.

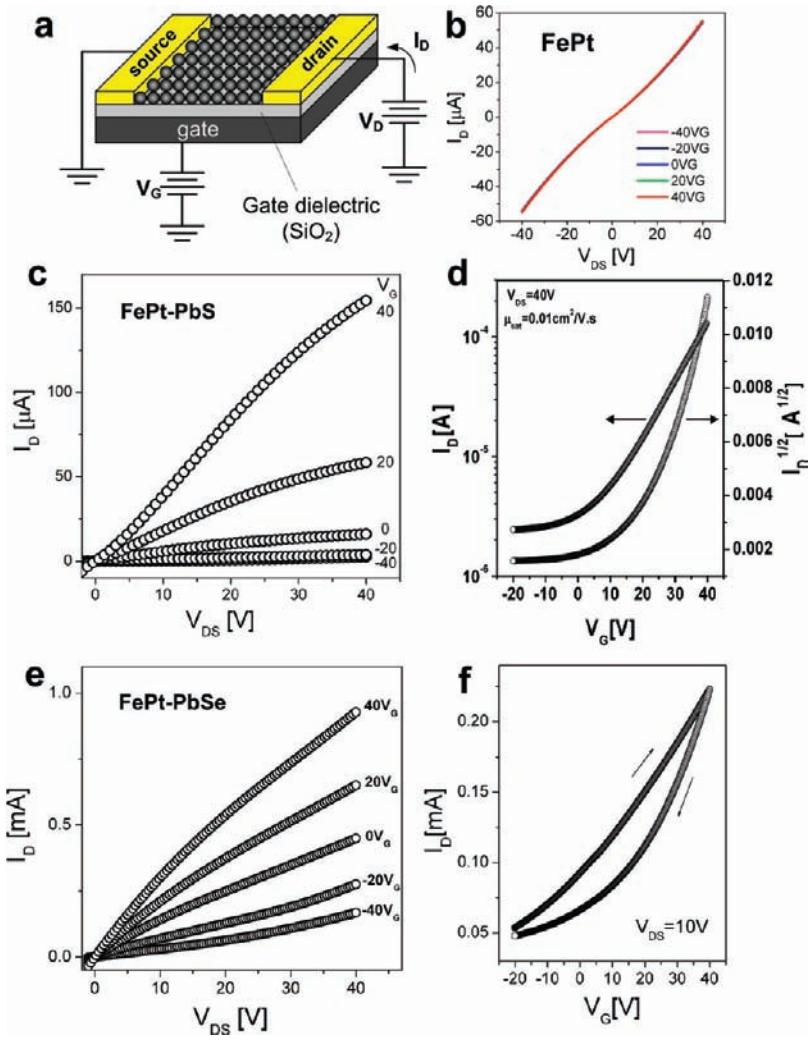

Figure 4. Gated n-type transport in FePt−PbS nanostructures. (a) Schematics of a field-effect transistor with a channel assembled of FePt−PbS nanostructures. (b) Drain current I_D plotted versus drain−source voltage V_{DS}, as a function of gate voltage V_G for an array of 3.5 nm FePt NCs. $L = 3$ μm, $W = 7500$ μm. (c) Plots of drain current I_D versus drain−source voltage V_{DS}, as a function of gate voltage V_G for FETs with channels assembled of FePt−PbS core−shell nanostructures. (d) Plots of I_D and $I_D^{1/2}$ vs V_G at constant $V_{DS} = 40$ V used to calculate the current modulation and field-effect mobility in the saturation regime for n-channel FET assembled from FePt−PbS core−shells. $L = 9.9$ μm, $W = 3800$ μm. (e) Drain current I_D plotted versus drain−source voltage V_{DS}, as a function of gate voltage V_G for a FET assembled from FePt−PbSe nanostructures. (f) Plot of I_D vs V_G at constant $V_{DS} = 10$ V used to calculate transconductance and linear field-effect mobility in the array of FePt−PbSe nanostructures.

the FePt alloy (φ_{FePt}) is ~5.0 eV,[28] while the electron affinity of bulk PbS is ~4.5 eV and even smaller for PbS NCs.[29] The φ_{FePt} may somewhat vary depending on the alloy composition; however, even if the above number is not accurate within a couple hundred meV, the FePt cores should trap the electrons added to the $1S_e$ state of the PbS shell. It is possible that dipoles formed at FePt/PbS and PbS/N_2H_4 interfaces affect the absolute positions of the energy levels in the core and the shell, respectively, in a way similar to how adsorbed dipolar molecules tune the work function of bulk metals.[30] Another possible explanation can be that the electron transport in arrays of FePt−PbS and FePt−PbSe nanostructures occurs via direct tunneling of electrons between the FePt cores through the PbS shells (Figure 5). As we show below, such long-distance tunneling is facilitated by the low effective mass of electrons in the PbS shell. The adsorption of electron-donating species like N_2H_4 lowers the energy barrier at the FePt−PbS interface compared to undoped nanostructures.[8]

The electron transfer rate from site A to site B ($\Gamma_{A\to B}$) can be generally expressed as:[31]

$$\Gamma_{A\to B} \approx g_A g_B \nu_0 \exp\{-2(2m^*\Delta E/\hbar^2)^{1/2}L\} \qquad (1)$$

where g_A and g_B are the numbers of occupied states in site A and unoccupied states in site B satisfying the conditions of resonant tunneling, ν_0 is the pre-exponential factor known as "attempt-to-escape frequency", m^* is the electron effective mass, and ΔE and L are the barrier height and width, respectively.

According to the Wentzel−Kramers−Brillouin (WKB) approximation, the probability of transmission through a complex

(28) Yin, C. K.; Murugesan, M.; Bea, J. C.; Oogane, M.; Fukushima, T.; Tanaka, T.; Kono, S.; Samukawa, S.; Koyanagi, M. *Jpn. J. Appl. Phys.* **2007**, *46*, 2167–2171.
(29) Hyun, B.-R.; Zhong, Y.-W.; Bartnik, A. C.; Sun, L.; Abrunifa, H. D.; Wise, F. W.; Goodreau, J. D.; Matthews, J. R.; Leslie, T. M.; Borrelli, N. F. *ACS Nano* **2008**, *2*, 2206–2212.
(30) de Boer, B.; Hadipour, A.; Mandoc, M. M.; van Woudenbergh, T.; Blom, P. W. M. *Adv. Mater.* **2005**, *17*, 621–625.
(31) Chandler, R. E.; Houtepen, A. J.; Nelson, J.; Vanmaekelbergh, D. *Phys. Rev. B* **2007**, *75*, 085325.

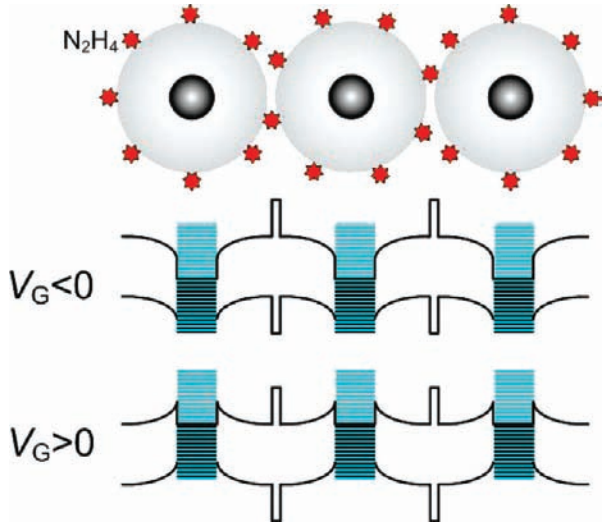

Figure 5. Proposed model for n-type transport and current modulation in arrays of FePt−PbS and FePt−PbSe nanostructures.

barrier can be written as the product of the probabilities of tunneling through the barrier components.[32] We calculated the exponential factor in eq 1 for the tunneling barrier consisting of two 4 nm thick PbS shells ($m^* = 0.085m_e$ and $\Delta E = 0.2$ eV) and a 0.4 nm thick layer of insulating ligands ($m^* = m_e$ and $\Delta E = 2$ eV[33]). It is usually accepted that the attempt-to-escape frequency ν_0 is approximately the same as the phonon frequency, typically $\sim 10^{13}$ s^{-1}. Metallic FePt cores provide much higher g_A and g_B compared to any quantum-confined semiconductor. 10^2 was used as a conservative estimate for $g_A g_B$ at room temperature. Substitution of these numbers to eq 1 provides an estimate for the charge transfer rate $\Gamma_{A\rightarrow B} \approx 7 \times 10^7$ s^{-1}.

To obtain an estimate for the macroscopic charge carrier mobility associated with this charge transport mechanism, we used modified Einstein relation $\mu = ed^2/(6k_BT\tau)$, where e is the electron charge, d is the hopping distance, k_B is the Boltzmann constant, T is the temperature, and τ is the hopping time inversely proportional to the tunneling rate.[34] A calculated low-field electron mobility of $\sim 6 \times 10^{-3}$ $cm^2/(V\ s)$ is in a good agreement with experimentally observed values, supporting the principal feasibility of the proposed n-type transport mechanism in the arrays of FePt−PbX (X = S, Se) nanostructures.

The modulation of current by applying gate potential is not possible for the films of 3.5 nm FePt NCs (Figure 4b). In the case of core−shell FePt−PbS nanostructures, applying positive V_G should lower the energy of the $1S_e$ state in PbS shells thus increasing the tunneling rate. In other words, every FePt−PbS−FePt junction in the current pass can be gated as shown in Figure 5.

Low-Temperature Charge Transport. FePt−PbX (X = S, Se) nanostructures showed a stable n-type gate effect under a nitrogen atmosphere at room temperature and ambient pressure. At the same time, exposure of samples to 10^{-6} Torr vacuum for 1 h switched the FETs from n-type to p-type as shown in Figure S12. Switching to the p-type transport has been previously observed in PbSe NC FETs,[8,19] and it was associated with desorption of N_2H_4 molecules. In that case p-type doping was provided by surface acceptor states located 50−70 meV above the $1S_h$ state of PbSe NCs.[35,36] To acquire additional information about charge transport in our nanostructures, we studied the temperature dependence of conductivity (G) for FePt−PbS and FePt−PbSe nanostructures (Figure 6a). The $I-V$ characteristics showed nearly ideal Ohmic behavior in the temperature range from 5 to 300 K, and G was measured under the low-bias conditions under constant driving current. The conductivity of FePt−PbS core−shells closely followed the $\ln G \propto T^{-1/2}$ dependence from 5 to 250 K (Figure 6a), which was previously observed in arrays of CdSe[37] and Au[38] NCs and explained by Efros−Shklovskii variable range hopping (ES-VRH)[39] and inelastic cotunneling, respectively. FePt−PbSe nanostructures showed a good linearity in the $\ln G$ vs $T^{-1/4}$ coordinates characteristic of Mott-type VRH.[40] The ES-VRH might be not applicable to FePt−PbSe nanostructures due to the larger dielectric constant of PbSe compared to PbS. At the same time, we want to emphasize that the theoretical framework developed for granular electronic systems[41,32] and used to describe the behavior of conventional NC solids[36,37,34,42] cannot be directly applied to multicomponent systems, and further theoretical and experimental studies will be required to fully understand this new class of materials. In some aspects, the electronic properties of multicomponent nanostructure arrays should resemble the properties of binary nanoparticles superlattices.[43]

The low-temperature measurements on FePt−PbX (X = S, Se) also revealed unusual features in the I_D vs V_G scans measured under constant V_{DS}. The NC FETs often show some hysteresis between V_G scans in the forward and reverse directions (Figure 6b). Such hysteresis is rather common for devices with thick gate dielectric layers and is typically associated with the charge trapping in the gate oxide or in the semiconductor channel.[19,44] We measured the evolution of I_D vs V_G scans with temperature and observed that below 260 K I_D changed with V_G not continuously but exhibiting an abrupt switching at a particular V_G (Figure 6b). Moreover, the hysteretic gate response reversed at low temperatures. Both current switching and hysteresis inversion originated from the presence of FePt cores since no similar effects were observed in the FETs assembled from PbS and PbSe NCs.[8,19] The hysteresis in the I_D-V_G scans measured for PbS and PbSe NC FETs was nearly temperature independent.

As discussed above, in the absence of n-type dopands like hydrazine, the Fermi energy of FePt should be close to the energy of the $1S_h$ state in the PbS shell. The features in the I_D

(32) Zabet-Khosousi, A.; Dhirani, A. A. *Chem. Rev.* **2008**, *108*, 4072–4124.
(33) Liljeroth, P.; Overgaag, K.; Urbieta, A.; Grandidier, B.; Hickey, S. G.; Vanmaekelbergh, D. *Phys. Rev. Lett.* **2006**, *97*, 096803–4.
(34) Yu, D.; Wang, C.; Guyot-Sionnest, P. *Science* **2003**, *300*, 1277–1280.
(35) Wang, R. Y.; Feser, J. P.; Lee, J. S.; Talapin, D. V.; Segalman, R.; Majumdar, A. *Nano Lett.* **2008**, *8*, 2283–2288.
(36) Mentzel, T. S.; Porter, V. J.; Geyer, S.; MacLean, K.; Bawendi, M. G.; Kastner, M. A. *Phys. Rev. B* **2008**, *77*, 075316.
(37) Yu, D.; Wang, C. J.; Wehrenberg, B. L.; Guyot-Sionnest, P. *Phys. Rev. Lett.* **2004**, *92*, 216802.
(38) Tran, T. B.; Beloborodov, I. S.; Lin, X. M.; Bigioni, T. P.; Vinokur, V. M.; Jaeger, H. M. *Phys. Rev. Lett.* **2005**, *95*, 076806.
(39) Shklovskii, B. I.; Efros, A. L. *Electronic Properties of Doped Semiconductors*; Springer-Verlag: Berlin, 1984.
(40) Mott, N. *Conduction in Non-Crystalline Materials*, 2nd ed.; Clarendon Press: Oxford, 1993.
(41) Beloborodov, I. S.; Lopatin, A. V.; Vinokur, V. M.; Efetov, K. B. *Rev. Mod. Phys.* **2007**, *79*, 469.
(42) Vanmaekelbergh, D.; Liljeroth, P. *Chem. Soc. Rev.* **2005**, *34*, 299–312.
(43) Shevchenko, E. V.; Talapin, D. V.; Kotov, N. A.; O'Brien, S.; Murray, C. B. *Nature* **2006**, *439*, 55–59.
(44) *Thin Film Transistors*; Kagan, C. R., Andry, P., Eds.; Marcel Dekker: New York, 2003.

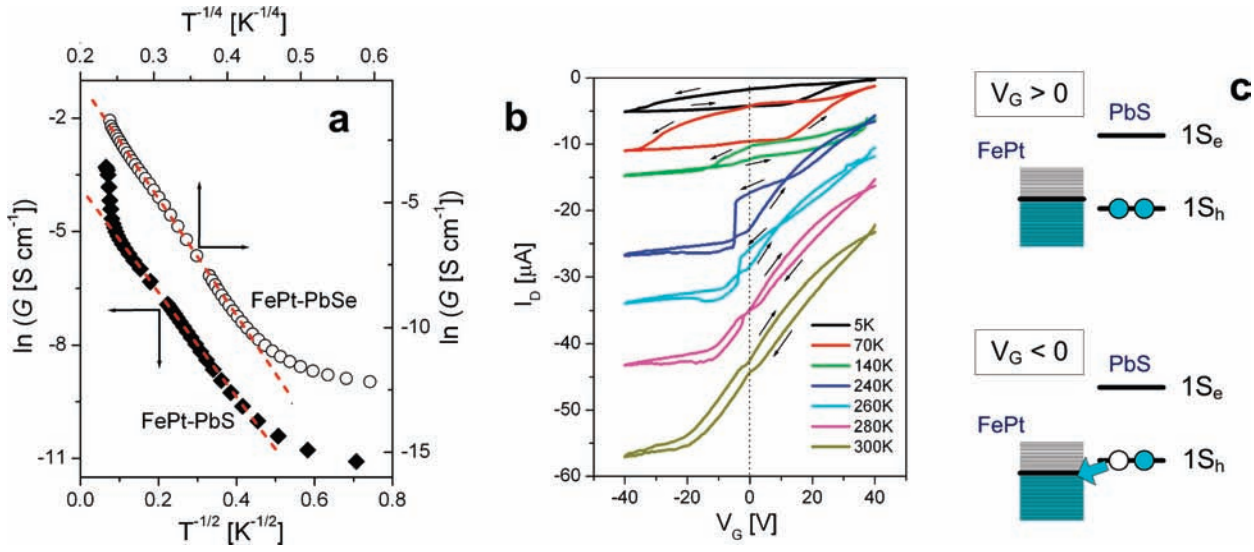

Figure 6. Temperature-dependent transport in FePt−PbX (X = S, Se) nanostructures. (a) The low-field conductance for a film of FePt−PbS core−shells plotted vs $T^{-1/2}$ (◆) and for a film of FePt−PbSe nanostructures plotted vs $T^{-1/4}$ (○). The linearities of ln G vs $T^{-1/2}$ and ln G vs $T^{-1/4}$ are characteristic of Efros−Shklovskii- and Mott-type variable range hopping transport of majority carriers (holes), respectively. (b) Plots of I_D vs V_G at constant $V_{DS} = -1$ V measured at different temperatures for FePt−PbS core−shells. (c) Gate- and temperature-dependent crossover of the highest occupied states in FePt−PbS nanostructures proposed to explain the features in I_D-V_G scans.

vs V_G scans shown in Figure 6b can be explained by changes in the relative alignment of the highest occupied electronic states in the core and in the shell of FePt−PbS nanostructures as schematically shown in Figure 6c. If the highest occupied state in the FePt core is higher in energy than the $1S_h$ state of the PbS shell, the FePt core will sink mobile holes from the PbS shell, lowering the film conductivity. In contrast, a negative bias applied to the gate terminal lifts the $1S_h$ of the PbS shell up in energy compared to the FePt core, and the nanostructures can form an intraparticle charge transfer complex as described in ref 19, providing additional doping to the PbS shell and increasing the conductivity (Figure 6c, bottom). At high temperature thermal broadening washes this effect out. The unusual temperature dependence of the band gap of the PbS shell (increasing with temperature, opposite to II−VI and III−V semiconductors) should also contribute to the stabilization of the charge-transfer complex at low temperatures. Similar, though less pronounced, effects of I_D switching and hysteresis reversal were observed for FePt−PbS dumbbells and FePt−PbSe nanostructures (Figures S13 and S14).

Magnetoresistance of FePt−PbS and FePt−PbSe Nanostructures. The ability to control electrical properties by an external magnetic field is used in the reading heads of hard drives and nonvolatile magnetoresistive random access memory (MRAM) devices. In addition, magnetotransport studies can provide important information on the role of electron spin in charge transport. We found that the films of both FePt−PbS and FePt−PbSe nanostructures showed strong negative magnetoresistance (i.e., decreased resistance with applied magnetic field). The magnetoresistance (MR) sign and the magnitude were independent of the direction of applied magnetic field (Figure S15). The MR measured for FePt−PbS core−shells (−14% at 5 K and 50 kOe) significantly exceeded the MR observed for an array of PbS nanocrystals (−0.2% at 5 K and 50 kOe) as shown in Figure 7a. FePt−PbSe nanostructures showed an even stronger MR, approximately −20% at 5 K and 50 kOe (Figure 7b). We did not observe MR saturation up to the 50 kOe field, so the effect should further increase with the increase in field strength. The MR amplitude decreased with temperature above 5 K, down to 3−5% at 20 K and nearly vanishing above 60 K.

Several mechanisms have been proposed to explain MR in different materials: so-called ordinary MR, wave function shrinkage, spin blockade, weak localization, spin-dependent tunneling (SDT), etc.[45] SDT has been previously observed in arrays of Co[46] and Fe_3O_4[47] NCs. Our experimental results also strongly point to SDT as the dominant MR mechanism in the arrays of FePt−PbX (X = S, Se) nanostructures. In favor of the SDT mechanism, the field dependences of MR measured at different temperatures above 5 K converged in a single master curve when plotted in coordinates of MR vs HT^{-1} (Figure 7c,d), predicted by the Inoue−Maekawa model[48] for a granular medium of magnetic particles with a random orientation of easy axes. The presence of disordered noncollinear surface spins, also observed in the magnetization of FePt−PbX (X = S, Se) nanostructures, explains the necessity of high fields to saturate MR.[24] The largest MR was observed at ∼5 K (Figure 7a,b). At lower temperatures MR dropped, saturating at −10% at high H. Such behavior can be explained by freezing disordered surface spins. The decrease of MR observed above 5 K can be caused by the spin-flip scattering processes often observed in the magnetic tunnel junctions.[46] The MR magnitude decreased with increasing applied bias, as typically observed in SDT[49] (Figure S16).

In SDT, the tunneling rate (Γ) between two NCs separated by an insulator can be expressed as

$$\Gamma = \Gamma_0(1 + P^2 \cos\theta) \qquad (2)$$

(45) Pippard, A. B. *Magnetoresistance in Metals*; Cambridge University Press: Cambridge, 1989.
(46) Black, C. T.; Murray, C. B.; Sandstrom, R. L.; Sun, S. *Science* **2000**, *290*, 1131–1134.
(47) Zeng, H.; Black, C. T.; Sandstrom, R. L.; Rice, P. M.; Murray, C. B.; Sun, S. *Phys. Rev. B* **2006**, *73*, 020402.
(48) Inoue, J.; Maekawa, S. *Phys. Rev. B* **1996**, *53*, R11927.
(49) Tsymbal, E. Y.; Mryasov, O. N.; LeClair, P. R. *J. Phys.: Condens. Matter* **2003**, *15*, R109–R142.

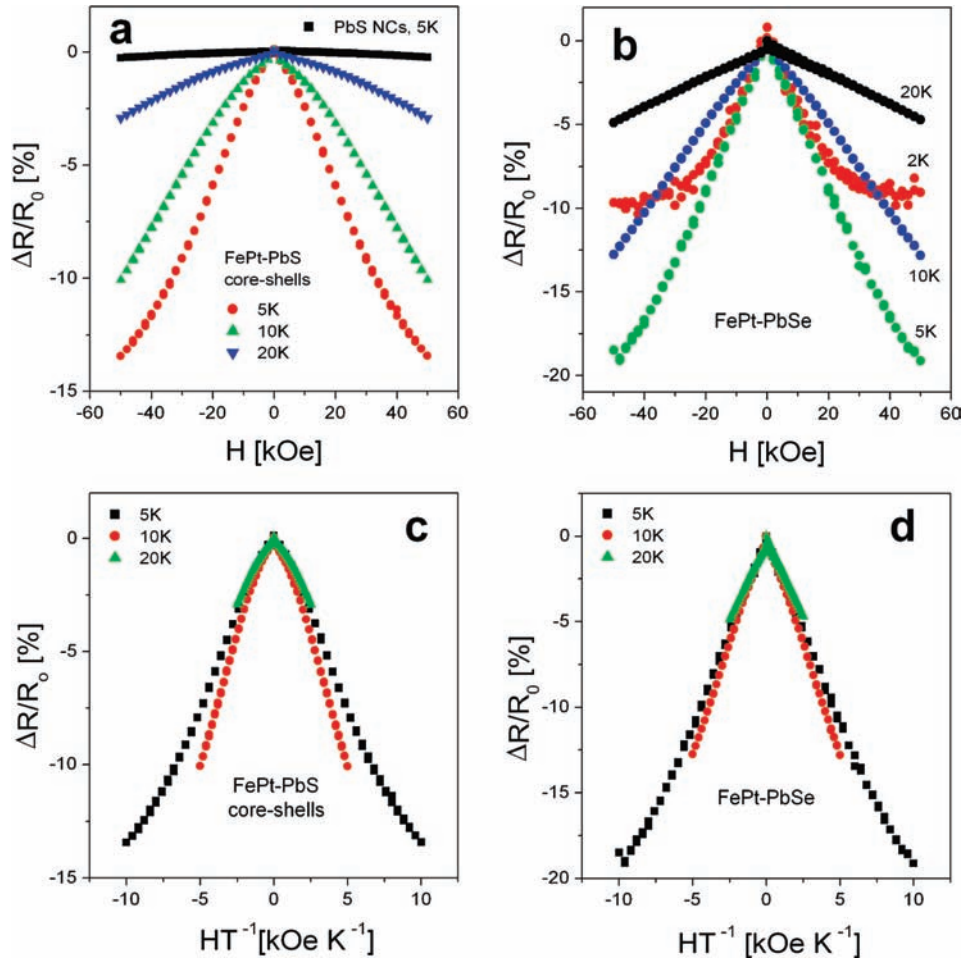

Figure 7. Magnetoresistance (MR) of FePt−PbX (X = S, Se) nanostructures. (a) Low-bias MR of FePt−PbS core−shells measured at different temperatures and compared to MR of a film of PbS nanocrystals. (b) Low-bias MR of FePt−PbSe nanostructures measured at different temperatures. (c,d) The field-dependences of MR measured at different temperatures converge in a master curve when plotted in coordinates MR vs HT^{-1} for (c) FePt−PbS and (d) FePt−PbSe nanostructures.

where Γ_0 is the spin-independent tunneling rate, θ is the angle between the magnetic moments in two NCs, and P is the electronic spin polarization of the material.[48] More explicitly, $P = (D_\uparrow - D_\downarrow)/(D_\uparrow + D_\downarrow)$, where $D_\uparrow$ and $D_\downarrow$ are the densities of electronic states at the Fermi energy for electrons with opposite spins. For the most realistic case of disordered magnetic moments θ takes a random value between 0 and π in the demagnetized state ($H = 0$). The maximum $\Delta R/R_0$ is then given by

$$MR = \Delta R/R_{max} = P^2/(1 + P^2). \quad (3)$$

According to Moriyama et al., P for FePt alloys depends on the degree of chemical order, increasing from ~0.24 for the chemically disordered fcc FePt phase to 0.38 for the $L1_0$ ordered alloy.[50] These values of P should lead to MR values ranging from 5.4% for a chemically disordered *fcc* phase to ~13% for the $L1_0$ phase. Our FePt cores had a chemically disordered phase, and the MR values observed for both FePt−PbS and FePt−PbSe nanostructures clearly exceed predicted values, thus pointing to some yet unknown contributions to MR in FePt−PbSe nanostructures. The cotunneling events with a synchronous movement of several electrons in a coordinated hopping event can increase the MR.[46,51] Spin polarization of the lead chalcogenide shell via exchange of charge carriers with the ferromagnetic core can also contribute to the observed MR effect.

4. Conclusions and Outlook

This work revealed synergistic behaviors in transport and magnetotransport properties of nanostructures combining semiconducting and magnetic components. Further developments should focus on the careful compositional and structural design required for achieving large MR, ideally at room temperature, combined with high carrier mobility and unique photophysics of quantum-confined semiconductors. For example, replacing the *fcc* FePt phase with the $L1_0$ phase with a much higher magnetocrystalline anisotropy and spin polarization or using half-metallic Fe_3O_4 cores could extend the temperature range of MR up to the range convenient for practical spin valves and other spintronic devices. Higher carrier mobilities could be achieved through proper design of organic or inorganic surface ligands.[52] With such improvements, chemically synthesized multifunctional nanostructures will be a source of rich new

(50) Moriyama, T.; Mitani, S.; Seki, T.; Shima, T.; Takanashi, K.; Sakuma, A. *J. Appl. Phys.* **2004**, *95*, 6789–6791.
(51) Takahashi, S.; Maekawa, S. *J. Magn. Magn. Mater.* **1999**, *198−199*, 143–145.
(52) Kovalenko, M. V.; Scheele, M.; Talapin, D. V. *Science* **2009**, *324*, 1417–1420.

physics and provide interesting opportunities for real-world device applications.

Acknowledgment. We thank M. Kovalenko, W. Heiss, I. Gruzberg, D. Vanmaekelbergh, and P. Guyot-Sionnest for stimulating discussions and B. Fisher and A. Belkin for help with magnetoresistance measurements. The work was supported by the NSF CAREER under Award Number DMR-0847535 and NSF MRSEC Program under Award Number DMR-0213745. M.I.B. acknowledges financial support from the Austrian Nanoinitiative (NSI). The work at the Center for Nanoscale Materials (ANL) was supported by the U.S. Department of Energy under Contract No. DE-AC02-06CH11357.

Supporting Information Available: Additional experimental details; TEM images of FePt−PbS nanostructures with different morphologies (Figures S1−S3). SAXS measured for FePt−PbS core−shell nanostructures (Figure S4). Characterization of magnetic properties of FePt−PbX (X = S, Se) nanostructures (Figures S5−S8). High-resolution SEM image of FET channel (Figure S9). Characteristics of FETs with channels assembled of FePt−PbX (X = S, Se) nanostructures (Figures S10−S14). Magnetoresistance measurements for FePt−PbS nanostructures (Figures S15, S16). This material is available free of charge via the Internet at http://pubs.acs.org.

JA100029S